PHYSICAL REVIEW D **80,** 125037 (2009)

General theory of oscillon dynamics

Marcelo Gleiser* and David Sicilia†

Department of Physics and Astronomy, Dartmouth College, Hanover, New Hampshire 03755, USA

(Received 2 November 2009; published 31 December 2009)

We present a comprehensive, nonperturbative analytical method to investigate the dynamics of time-dependent oscillating scalar field configurations. The method is applied to oscillons in a ϕ^4 Klein-Gordon model in two and three spatial dimensions, yielding high accuracy results in the characterization of all aspects of the complex oscillon dynamics. In particular, we show how oscillons can be interpreted as long-lived perturbations about an attractor in field configuration space. By investigating their radiation rate as they approach the attractor, we obtain an accurate estimate of their lifetimes in $d = 3$ and explain why they seem to be perturbatively stable in $d = 2$, where d is the number of spatial dimensions.

DOI: 10.1103/PhysRevD.80.125037 PACS numbers: 11.27.+d, 03.65.Pm, 05.45.Yv

I. INTRODUCTION

Nonlinear field theories contain a large number of localized solutions that display a rich array of properties [1]. Of particular interest are those that are static and stable, that is, that retain their spatial profile as they move across space or scatter with each other, as is the case of sine-Gordon solitons. The details of the solitonic configurations are, of course, sensitive to the dimensionality of space and to the nature of the field interactions. Long ago, Derrick has shown that, in the case of models with just a real scalar field, no static solitonic configurations can exist in more than one spatial dimension [2]. Given that most models of interest in high energy physics involve more complicated fields in three spatial dimensions, this restriction was somewhat frustrating. Fortunately, the subsequent exploration of a variety of models led to a plethora of static, nonperturbative, localized field configurations. Examples include topological defects, solutions of models usually involving gauge fields that owe their stability to the nontrivial topology of the vacuum, such as strings and monopoles [3], and the so-called nontopological solitons, solutions of models where a conserved global charge is trapped inside a finite region of space due to a mass gap condition, such as Q-balls [4] and the models with a real and a complex scalar field of Friedberg, Lee, and Sirlin [5].

In the midnineties [6], a new class of localized nonperturbative solution began to be explored in detail, after being proposed earlier [7]. Named oscillons, such long-lived solutions have the distinctive and counter-intuitive feature of being time-dependent. In spite of this, the nonlinear interactions act to preserve the localization of the energy, which remains approximately constant for a surprisingly long time [8]. During the past few years, oscillons have attracted much interest. Their properties were explored in two [9] and higher [10] spatial dimensions, in the presence of gauge fields [11], in the standard model of particle physics [12], and in a simple cosmological setting [13]. There have also been detailed attempts at understanding some properties of oscillon-related configurations (typically with small-amplitude oscillations), including their longevity, using perturbative techniques [14]. On the other hand, a treatment explaining the remarkable longevity of oscillons in models related to spontaneous symmetry breaking, and thus of obvious interest in particle physics and cosmology, has been lacking. The situation was partially remedied recently, when we published a preliminary treatment of the problem [15]. In the present work, we greatly extend the range of our dynamical theory of oscillons in scalar field models, include the details of many key derivations, and demonstrate its accuracy in reproducing numerical results. Our approach is general enough to be extended to different scalar field models that exhibit long-lived, time-dependent localized configurations.

II. LINEAR VS. NONLINEAR DYNAMICS AND THE OSCILLON MASS GAP

In order to introduce some of the basic quantities needed for our theory, it is instructive to start by reviewing some of the main properties of relativistic oscillons. We will do so in the context of a simple ϕ^4 model with a symmetric double-well potential, as this is also the main focus of the present work. To begin, consider the Lagrangian for a spherically-symmetric, real scalar field in d-spatial dimensions,

$$L = c_d \int r^{d-1} dr \left[\frac{1}{2}\dot{\phi}^2 - \frac{1}{2}\left(\frac{\partial \phi}{\partial r}\right)^2 - V(\phi) \right], \quad (1)$$

where $V_0(\phi) = m^2\phi^2 + V_{\rm NL}$, and $c_d = 2\pi^{d/2}/\Gamma(d/2)$ is the unit-sphere volume in d dimensions. $V_{\rm NL}$ represents the nonlinear terms to the potential, which we will add later on. Quantities are scaled to be dimensionless as follows: $\phi = m^{(d-1)/2}\phi_0$ and $r^\mu = r_0^\mu/m$. We will henceforth only use dimensionless variables, dropping the subscript "0."

*mgleiser@dartmouth.edu
†davidovich@dartmouth.edu

We start by investigating the linear theory [$V_{\rm NL} = 0$ in Eq. (1)] so that we can more easily contrast it with nonlinear models that give rise to oscillons. Since oscillons have been shown to maintain their approximate Gaussian-shaped spatial profiles during their lifetimes, we will write the scalar field as

$$\phi(r, t) = A(t)P(r; R) = A(t)e^{-r^2/R^2}. \quad (2)$$

Here, $A(t)$ is the time-dependent amplitude of the configuration and $P(r; R)$ its spatial profile, which is parameterized by the radial extension R.

A. Linear dynamics

As shown in Ref. [8], the $d = 3$ linear theory with a Gaussian-profile initial condition has the solution,

$$\phi(r, t) = \frac{R^3}{2}\frac{A}{\sqrt{\pi}}\int_0^\infty k e^{-R^2k^2/4}\frac{\sin(kr)}{r}\cos(\omega t)dk, \quad (3)$$

where A is an arbitrary initial amplitude and the dispersion relation is $\omega = (k^2 + \omega_{\rm mass}^2)^{(1/2)}$, where the mass frequency $\omega_{\rm mass} = \sqrt{2}$. To calculate $\Gamma_{\rm lin}$, the decay width associated with the above solution, we recall that in [8] it was also shown that Eq. (3) can be approximately integrated to obtain (at $r = 0$, the configuration's maximum amplitude)

$$\phi(0, t) = \frac{A_0}{(1 + \frac{2t^2}{R^4})^{(3/4)}}\cos\left(\sqrt{2}t + \frac{3}{2}\tan^{-1}\left[\frac{\sqrt{2}t}{R^2}\right]\right), \quad (4)$$

whose envelope of oscillation is given by $\phi(0, t) = A_0/(1 + 2t^2/R^4)^{3/4}$, which reaches $1/e$ of its initial value in a time given by $\mathcal{T}_{\rm linear} \simeq .836\omega_{\rm mass}R^2$. This yields the linear decay width $\Gamma_{\rm lin}$,

$$\frac{1}{2}\Gamma_{\rm lin} = \frac{1}{\mathcal{T}_{\rm linear}} \simeq \frac{1.196}{\omega_{\rm mass}R^2} \simeq \frac{.846}{R^2}. \quad (5)$$

In the linear theory, any initial configurationor excitation above the vacuum-will quickly decay by emitting radiation. The key difference between the linear and the oscillon-supporting nonlinear models is that, in the latter case, the decay modes are strongly suppressed. It is this suppression that gives rise to the oscillon's remarkable longevity. Our goal in this paper is to make this statement quantitatively precise. To obtain the linear radiation distribution, which we denote by $b(\omega)$, we simply take the k-space representation $ke^{-R^2k^2/4}$ of the Gaussian in Eq. (3) and express it in terms of ω using the dispersion relation $\omega = (k^2 + 2)^{(1/2)}$:

$$b(\omega) = k[\omega]e^{-R^2k[\omega]^2/4} = (\omega^2 - 2)^{(1/2)}e^{-R^2(\omega^2-2)/4}. \quad (6)$$

$b(\omega)$ is a lopsided distribution with frequencies above $\omega_{\rm mass} = \sqrt{2}$ and peaked at $\omega_{\rm max} = (2 + 2/R^2)^{1/2}$. Now define $\omega_{\rm left}$ and $\omega_{\rm right}$ to be the frequencies where the distribution $b(\omega)$ rises to half of its peak value. A straightforward calculation gives $\omega_{\rm left} \simeq (2 + .203/R^2)^{(1/2)}$ and $\omega_{\rm right} \simeq (2 + 7.38/R^2)^{(1/2)}$. The radiation distribution is then approximately centered on the frequency $\omega_{\rm lin}$, given by (see Fig. 1)

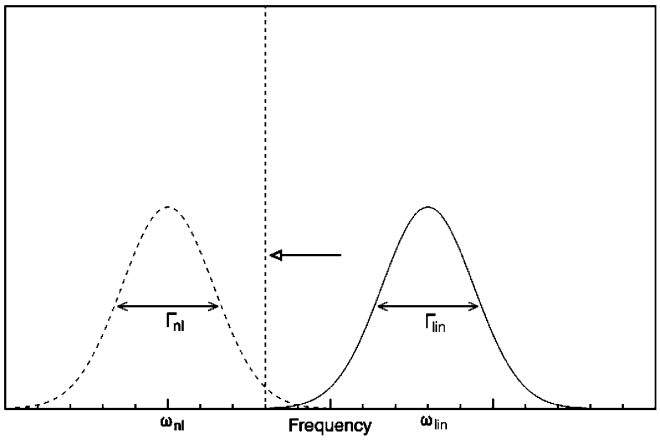

FIG. 1. Schematic description of the linear radiation peak centered on $\omega_{\rm lin}$ being shifted to the left by the presence of nonlinearities. An oscillon will form if the peak is shifted far enough into the nonlinear region such that it no longer overlaps significantly with the linear peak.

$$\omega_{\rm lin} \equiv \frac{1}{2}(\omega_{\rm left} + \omega_{\rm right}) \simeq \frac{1}{2}\left(2 + \frac{.203}{R^2}\right)^{(1/2)} + \frac{1}{2}\left(2 + \frac{7.38}{R^2}\right)^{(1/2)}, \quad (7)$$

which we take to represent the dominant linear radiation frequency.

B. Nonlinear dynamics and decay rate

Imagine now that one or more nonlinear terms are added to the linear potential and that the field is again initialized with the same localized Gaussian perturbation. Roughly speaking, the nonlinearities will shift the dominant linear oscillation frequency $\omega_{\rm lin}$, to a new value, denoted by $\omega_{\rm nl}$. If the added terms serve to decrease the curvature of the potential, then $\omega_{\rm nl} < \omega_{\rm lin}$. Such a situation is depicted qualitatively in Fig. 1, where the arrow indicates how the shift in frequencies occurs.

When nonlinearities are efficient enough that $\omega_{\rm nl}$ is lowered substantially below $\omega_{\rm lin}$, an oscillon may form. The reason for this is the following. As the initial field configuration begins to oscillate, it will attempt to emit small-amplitude radiation waves in an effort to dissipate its energy. However, if $\omega_{\rm nl}$ is sufficiently less than $\omega_{\rm lin}$, the bulk of the frequency components composing the oscillation will be unable to excite small-amplitude radiation waves (since the configuration can only radiate appreciably in the frequency range $\omega_{\rm left} < \omega < \omega_{\rm right}$). This condition leads to the stabilization mechanism responsible for the formation of oscillons.

It then follows that the oscillon will enter the nonlinear regime if the two peaks in Fig. 1 do not significantly overlap. Mathematically, the right "edge" of the nonlinear peak, given by $\omega_{\rm nl} + \frac{1}{2}\Gamma_{\rm nl}$, must be less than the left edge of the linear peak, given by $\omega_{\rm lin} - \frac{1}{2}\Gamma_{\rm lin}$. Therefore, we have $\omega_{\rm nl} + \frac{1}{2}\Gamma_{\rm nl} < \omega_{\rm lin} - \frac{1}{2}\Gamma_{\rm lin}$ which, by defining $\omega_{\rm gap} \equiv \omega_{\rm lin} - \omega_{\rm nl}$ as the frequency gap between the linear and nonlinear peaks, becomes

$$\omega_{\rm gap} > \frac{1}{2}(\Gamma_{\rm nl} + \Gamma_{\rm lin}). \tag{8}$$

Since nonlinearities tend to increase a configuration's lifetime and thus decrease its decay rate, it follows that $0 \leq \Gamma_{\rm nl} \leq \Gamma_{\rm lin}$. One can thus state that if

$$\omega_{\rm gap} > \Gamma_{\rm lin}, \tag{9}$$

then the configuration will be forced into the nonlinear regime. In other words, Eq. (9) is a *necessary* condition for the formation of an oscillon. As we will soon see, if an oscillon is formed and, during the course of its time evolution, reaches a point where Eq. (9) is no longer satisfied, it will cease to exist. This implies that oscillons decay when

$$\omega_{\rm gap} = \Gamma_{\rm lin}. \tag{10}$$

To obtain the nonlinear radiation frequency $\omega_{\rm nl}$ and thus $\omega_{\rm gap}$, we substitute Eq. (2) into Eq. (1) and integrate, giving

$$\begin{aligned} L &= \left(\frac{\pi}{2}\right)^{(d/2)} R^d \left[\frac{1}{2}\dot{A}^2 - V(A_{\rm max})\right]; \\ E &= \left(\frac{\pi}{2}\right)^{(d/2)} R^d V(A_{\rm max}), \end{aligned} \tag{11}$$

where $V(A)$ now includes nonlinear terms and E is the energy which is found by taking the appropriate Legendre transform of the Lagrangian and evaluating it at the upper turning point of an oscillation, $A_{\rm max}$. The oscillation frequency of the oscillon, $\omega_{\rm nl}$, at a given time is given by

$$\frac{2\pi}{\omega_{\rm nl}} = \mathcal{T}_{\rm osc} = \int_0^{\mathcal{T}_{\rm osc}} dt = 2\int_{A_{\rm max}}^{A_{\rm min}} \frac{dA}{\dot{A}}, \tag{12}$$

where $\dot{A} = [2E/c_R - 2V(A)]^{1/2}$, $c_R \equiv (\pi/2)^{d/2}R^d$, and $A_{\rm min}$ is given by $V(A_{\rm min}) = V(A_{\rm max})$.

C. The attractor point

Results from numerical simulations suggest that there exists an attractor point in configuration space to which the oscillon tends. It was noted in [15] that one can obtain the energy of this attractor point (in ϕ^4 models) by finding the minimum energy which has the property that the effective potential $V(A)$ possesses at least one point for which $V''(A) \leq 0$. In order to compute the attractor point, it is easier to work within a specific model. Choosing $V_0(\phi) = \phi^2 - \phi^3 + \phi^4/4$, we obtain, using Eq. (2) and integrating over all space,

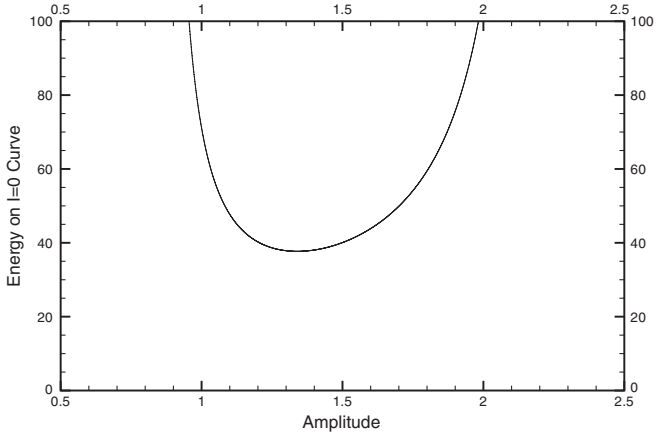

FIG. 2. Minimum oscillon energy as a function of core amplitude for a double-well potential in $d = 3$. The minimum of this curve is the attractor point with $E_\infty \simeq 37.69$.

$$V(A) = \left(1 + \frac{d}{2R^2}\right)A^2 - \left(\frac{2}{3}\right)^{(d/2)}A^3 + \frac{A^4}{2^{((d+4)/(2))}}, \tag{13}$$

and

$$V''(A) = \left(2 + \frac{d}{R^2}\right) - 6\left(\frac{2}{3}\right)^{(d/2)}A + 3\frac{A^2}{2^{(d/2)}}. \tag{14}$$

Equate this to zero and solve for R as a function of A. Then substitute the result into Eq. (11) to eliminate R, yielding energy as a function only of A. This curve possesses a *minimum*, shown in Fig. 2 for $d = 3$, the energy of which yields the correct attractor energy E_∞ of the oscillon, which has numerical values $E_\infty \simeq 4.44$ in $d = 2$ and $E_\infty \simeq 37.69$ in $d = 3$.

Given the energies calculated above, there is a locus of points in (A, R) parameter space (the thinner solid lines in Figs. 3 and 4) which possess these asymptotic values for the energy; one of them is the attractor. To locate the attractor point, we need to determine its amplitude coordinate, denoted A_∞. In $d = 2$, this is most easily determined numerically to be $A_\infty \simeq .3$. In $d = 3$, we cannot determine A_∞ numerically since the oscillon decays before reaching it. Therefore, in $d = 3$, we must estimate A_∞ analytically. To do this, we choose the point (satisfying $E = E_\infty$) which has $\omega_{\rm nl} \simeq \omega_{\rm mass}$, even though, in reality, its frequency is slightly less than $\omega_{\rm mass}$ (never above it). As we will see, this approximation will suffice for our purposes. From Eq. (12), the amplitude which gives $\omega_{\rm nl} \simeq \omega_{\rm mass}$ (in $d = 3$) has numerical value $A_\infty \simeq .456$.

Given the pair $(A_\infty, E_\infty) \simeq (.456, 37.69)$ in $d = 3$ and $(A_\infty, E_\infty) \simeq (.3, 4.44)$ in $d = 2$, we can use Eq. (11) to obtain R_∞. We obtain $R_\infty \simeq 4.79$ for $d = 3$, and $R_\infty \simeq 5.77$ in $d = 2$. The circles in Figs. 3 ($d = 3$) and 4 ($d = 2$) mark the locations of the attractor points.

Given Eqs. (5), (7), and (12) (and their equivalents in $d = 2$ shown in Appendix A), we can also calculate the quantities in Eq. (9), that is, the oscillon existence condi-

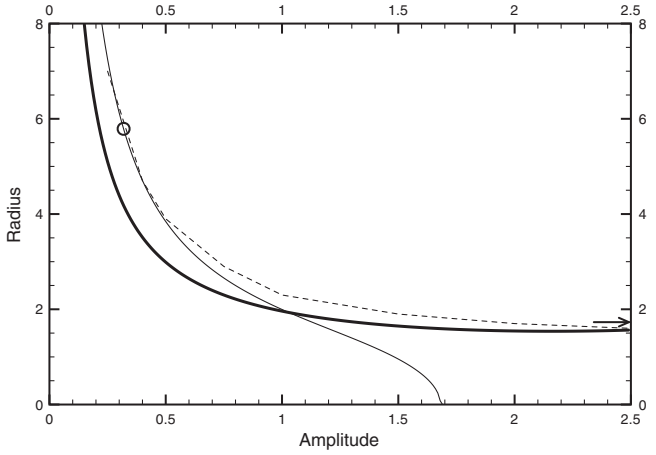

FIG. 3. The thick solid line represents the locus of points satisfying the condition $\omega_{\rm gap} = \Gamma_{\rm lin}$ in $d = 2$ (''line of existence'') calculated analytically. The thin solid line represents the locus of points that have the attractor energy $E \simeq 4.44$. The dashed line is the numerical minimum radius based on Gaussian initial configurations. Oscillons can only exist if their energy $E \geq E_\infty$ and if they have a core amplitude and average radius lying above the line of existence. This is why the numerically measured minimum radius follows the line of existence for $A \gtrsim 1$ but follows the line of minimum energy for $A \lesssim 1$. The arrow indicates the value of the (constant) minimum radius calculated in [8]. The circle represents the location of the attractor point; since it lies above the line of existence, oscillons will be perturbatively stable in this system.

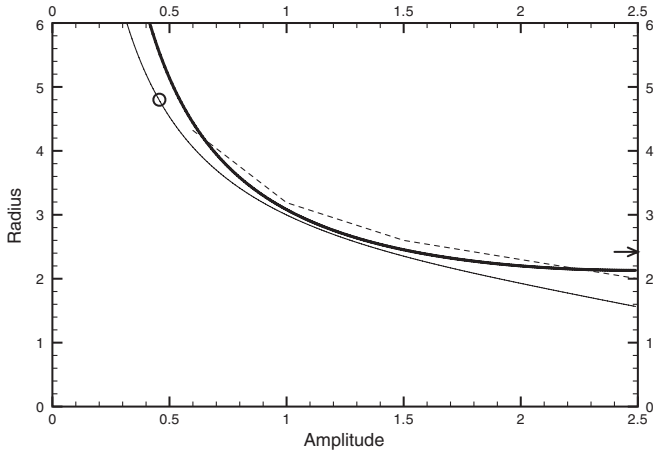

FIG. 4. The thick solid line represents the locus of points satisfying the condition $\omega_{\rm gap} = \Gamma_{\rm lin}$ in $d = 3$ (line of existence) calculated analytically. The thin solid line represents the locus of points that have the attractor energy $E \simeq 37.69$. The dashed line is the numerical minimum radius based on Gaussian initial configurations. The arrow indicates the value of the (constant) minimum radius calculated in [8]. Oscillons can only exist if their core amplitude and average radius are above the curve (wherein $E \geq E_\infty$ is automatically satisfied). The circle represents the location of the attractor point; since it lies below the line of existence, oscillons will not be absolutely stable in this system.

tion, as a function of the parameter pair (A, R). In Figs. 3 ($d = 2$) and 4 ($d = 3$), the thicker continuous lines represent the locus of points satisfying $\omega_{\rm gap} = \Gamma_{\rm lin}$, defining the boundary line between the region where oscillons may exist (above the line, and provided that $E > E_\infty$) and where they cannot exist (below the line). We will often refer to this boundary as the ''line of existence.'' As a test of the existence condition [Eq. (9)], we also plot the numerical result for the ''minimum radius'' as a function of amplitude (dashed line), found by pinpointing the minimum initial radius which causes a configuration to live longer than the linear decay time. The arrows in Figs. 3 and 4 indicate the values of the minimum radii calculated in [8] which possess no amplitude dependence and thus provide only limited information.

As can be seen, the attractor point in $d = 3$ lies *below* the line of existence curve, explaining the finite lifetimes of oscillons in that system: the configurations decay before reaching the attractor point. On the other hand, the attractor point in $d = 2$ lies *above* the curve, explaining the seemingly infinite oscillon lifetimes observed in numerical simulations. We can thus interpret the oscillons as time-dependent perturbations about the attractor point. Those in $d = 3$ are unstable, albeit some can be extremely long-lived. Those in $d = 2$ are at least perturbatively stable.

In situations such as $d = 3$, where oscillons eventually decay, it is interesting to compute their lifetimes and how they depend on their radiation rate. In a recent work, we presented the basic features of a method designed to do so [15]. In the next section, we develop the appropriate formalism in detail, based on the overlap between the nonlinear and linear radiation spectra. We point out that our formalism is, in principle, applicable to any time-dependent scalar field configuration, offering a much-needed handle on how to compute radiation rates of non-perturbative configurations in relativistic scalar filed theories.

III. LIFETIME OF LONG-LIVED OSCILLONS: GENERAL THEORY

In the situation that $\omega_{\rm gap} > \Gamma_{\rm lin}$ and an oscillon has formed (above the solid curve in Fig. 4) it will begin to radiate small amounts of energy. In this section, we will derive a general equation governing its radiation rate so that, in the event that $\omega_{\rm gap} = \Gamma_{\rm lin}$ and the oscillon decays, we may calculate its lifetime. As in the previous section, our general approach will be to compute the overlap between the nonlinear peak and the linear peak. Since we are assuming that $\omega_{\rm gap} > \Gamma_{\rm lin} \gg \Gamma_{\rm nl}$ for a long-lived oscillon, this overlap will be small; the amount by which it differs from zero will determine the radiation rate.

In Fig. 5, we plot a possible frequency distribution for an oscillon (the width of the peak centered on $\omega_{\rm nl}$ has been greatly exaggerated for visibility) in units of the mass frequency ($\omega_{\rm mass} = \sqrt{2}$). Note how the tail of the distribu-

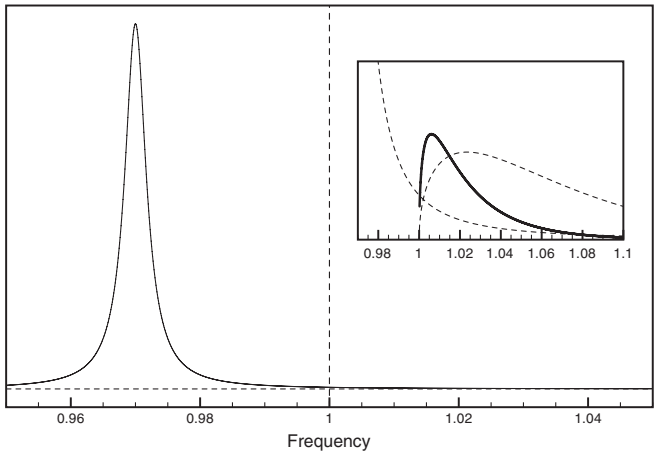

FIG. 5. Schematic of an oscillon frequency distribution showing the tail penetrating the radiation region. The graph is plotted in units of $\omega_{\rm mass}$. In the inset we show a close-up view of $\mathcal{F}(\omega)$ and $b(\omega)$, respectively, (dashed lines), and their product $\Omega(\omega)$ (solid line) for the system given by Eq. (1) in $d = 3$ for typical values of the various parameters. Note that the curves have been vertically scaled so that all are visible on the same graph.

tion "leaks" beyond the mass frequency. It is this leakage that will determine the radiation rate and thus the decay rate of the oscillon.

A. The long-lived oscillon radiation equation

In order to compute the oscillon decay rate, we model oscillons as spherically-symmetric objects whose radiation obeys a distribution (amplitude per unit frequency) $\Omega(\omega)$ which consists of a narrow peak of width δ centered at some frequency $\omega_{\rm rad}$. The radiation flux Φ (energy per unit time per unit surface area) emitted by such an object is

$$\Phi \equiv -\frac{\dot{E}}{S} \simeq \rho v \simeq \frac{1}{2}\mathcal{A}^2\omega_{\rm rad}^2\frac{\omega_{\rm rad}}{k_{\rm rad}} \simeq \frac{1}{2}\delta^2\Omega(\omega_{\rm rad})^2\frac{\omega_{\rm rad}^3}{k_{\rm rad}}, \tag{15}$$

where S is the surface area of the oscillon, ρ is the radiation-wave energy density, $v = \omega_{\rm rad}/k_{\rm rad}$ is the phase velocity of the wave, $k_{\rm rad}$ is the wave number, and $\mathcal{A}$ is the amplitude of the radiation wave, which is given by

$$\mathcal{A} = \int_{\omega_{\rm mass}}^{\infty} \Omega(\omega)d\omega \simeq \Omega(\omega_{\rm rad})\delta. \tag{16}$$

The function $\Omega(\omega)$, which represents the amplitude per unit frequency of the radiation wave, is simply determined by the "overlap" between the oscillon and the linear radiation peaks. Taking $\Omega(\omega)$ (the *overlap function*) to be the product of the nonlinear peak and the linear radiation distribution $b(\omega)$ obtained in the previous section, we have

$$\Omega(\omega) = \alpha\mathcal{F}(\omega)b(\omega); \qquad \equiv \mathcal{F}(\omega)\tilde{b}(\omega), \tag{17}$$

where $\mathcal{F}(\omega)$ is the nonlinear peak (Fourier transform of the oscillon's core). α is a proportionality constant to be determined, and $\tilde{b} \equiv \alpha b(\omega)$. The inset in Fig. 5 shows a typical overlap function for an oscillon in $d = 3$. (See Appendix C for details.) In Appendix B we show that, in the tail,

$$\mathcal{F}(\omega) \simeq -\sqrt{\frac{2}{\pi}}\frac{\dot{A}}{1+\chi}(\omega - \omega_{\rm nl})^{-2}. \tag{18}$$

Combining Eqs. (15), (17), and (18) and letting $S = c_d R^{d-1}$, we have

$$\eta\frac{dE}{dt} + \left(\frac{dA}{dt}\right)^2 = 0, \tag{19}$$

where η is a time-dependent parameter given by

$$\eta \equiv \frac{\pi(1+\chi)^2(\omega_{\rm rad} - \omega_{\rm nl})^4 k_{\rm rad}}{c_d R^{d-1}\omega_{\rm rad}^3\delta^2\tilde{b}(\omega_{\rm rad})^2}. \tag{20}$$

Equation (19) is a differential equation which must be satisfied by a long-lived oscillon. In Appendix C, we compute both α and δ in general and in the context of the model of Eq. (1).

B. Integration of the long-lived oscillon radiation equation

In this section, we will attempt to integrate Eq. (19) to obtain the oscillon energy as a function of time. This process is not straightforward since Eq. (19) contains derivatives of two different quantities (amplitude and energy) and the parameter η possesses a complicated time dependence which is not known. However, in Appendix D we develop a simple method to solve this problem, based on the assumption that the time scale associated with the oscillon's loss of energy is closely related to the time scales associated with the rates of change of all other oscillon parameters. The result of our approach is Eq. (D4), which we will employ below.

First, write Eq. (D4) for the cases $X = A$ and $X = \eta$ and substitute into Eq. (19), obtaining,

$$\dot{E} = \frac{-1}{\rho_A^2\gamma_A^2}[\eta_\infty + \gamma_\eta(E - E_\infty)^{\rho_\eta}](E - E_\infty)^{2-2\rho_A}. \tag{21}$$

Now, consider the situation where $\eta_\infty \simeq 0$ (which is the case in the system we are studying here since, in $d = 3$, the attractor point satisfies $\omega_{\rm nl} \simeq \omega_{\rm mass}$, leading to $\omega_{\rm rad} \simeq \omega_{\rm mass}$, which causes η to be zero there). In this situation, Eq. (21) is somewhat simplified:

$$\dot{E} = -\gamma_{\dot{E}}(E - E_\infty)^{\rho_{\dot{E}}}, \tag{22}$$

where the constant $\gamma_{\dot{E}}$ is given by

$$\gamma_{\dot{E}} \equiv \frac{\gamma_\eta}{\rho_A^2\gamma_A^2}, \tag{23}$$

and the exponent $\rho_{\dot{E}}$ is (using that $[\dot{E}]_\infty = 0$)

$$\rho_{\dot{E}} = 2(1 - \rho_A) + \rho_\eta. \tag{24}$$

Equation (22) is a constant-coefficient, ordinary differential equation governing the oscillon energy as a function of time, and can be easily integrated:

$$E(t) = E_\infty + \frac{E_i - E_\infty}{[1 + \gamma_{\dot{E}} g (E_i - E_\infty)^g t]^{(1/g)}}, \tag{25}$$

where $g \equiv \rho_{\dot{E}} - 1$ and E_i is the energy at $t = 0$. Equation (25) is the energy of an oscillon as a function of time.

As shown in Fig. 4, in $d = 3$ an oscillon will always decay before reaching $E = E_\infty$. The decay is quite sudden, a burst of scalar radiation. As stated in Sec. II, this occurs when $\omega_{\rm gap} = \Gamma_{\rm lin}$; hence the decay energy, denoted E_D, is given by

$$E_D = E|_{[\omega_{\rm gap} = \Gamma_{\rm lin}]}. \tag{26}$$

To calculate the lifetime, denoted $\mathcal{T}_{\rm life}$, which is defined as the amount of time taken for the oscillon to decay from a sufficiently high initial energy down to E_D, we invert Eq. (25) to yield time as a function of energy and evaluate at E_D:

$$t(E_D) = \frac{1}{\gamma_{\dot{E}} g}\left[\frac{1}{(E_D - E_\infty)^g} - \frac{1}{(E_i - E_\infty)^g}\right]. \tag{27}$$

When $E_i - E_\infty \gg E - E_\infty$, the function $t(E)$ tends to a finite, maximum value leading to

$$\mathcal{T}_{\rm life} = \frac{1}{\gamma_{\dot{E}} g} \frac{1}{[E_D - E_\infty]^g}. \tag{28}$$

This means that, when the initial energy E_i is much larger than the energy E_D in question, the time it takes for $E(t)$ to fall from E_i to E_D becomes independent of the initial condition (i.e., from E_i). One can then say that, in a restricted sense, the long-lived oscillon is decoupled from initial conditions: if the necessary conditions for its existence are satisfied, a variety of initial configurations will approach an oscillon. Recent studies that have observed the emergence of oscillons from stochastic initial conditions after a fast quench offer strong support for this claim [16].

Equations (26) and (28) together give the lifetime of an oscillon and can be considered the main results of this paper. Before moving on, we note that, for a long-lived oscillon, $\Gamma_{\rm nl}$ is given by

$$\Gamma_{\rm nl} \equiv \Gamma_A = -\frac{\dot{A}}{A - A_\infty} = -\rho_A \frac{\dot{E}}{E - E_\infty} = \rho_A \gamma_{\dot{E}} (E - E_\infty)^g, \tag{29}$$

where we have used Eqs. (B9), (D3), and (22). This is related to the lifetime by [combine Eqs. (28) and (29)]

$$\mathcal{T}_{\rm life} = \left(\frac{\rho_A}{g}\right)\Gamma_{\rm nl}^{-1}|_{E=E_D}. \tag{30}$$

C. Sample calculation: ϕ^4 Klein-Gordon field in $d = 3$

We now apply the above results to the system given by the Lagrangian in Eq. (1) for $d = 3$, supplemented by the nonlinear potential of Eq. (13). We will begin with the existence condition shown in Fig. 4. In Sec. II C, we calculated the coordinates of the attractor point and obtained $(A_\infty, R_\infty) \simeq (.456, 4.79)$. Comparison with Fig. 4 reveals that the attractor point lies below the curve, and thus that $\omega_{\rm gap}/\Gamma_{\rm lin} < 1$ there. As we noted before, stable oscillons will not exist in this model. However, there are still long-lived oscillons obtained by initializing the field sufficiently far from the attractor point.

As these structures radiate energy, their amplitude A and radius R will change in time. Hence, they will trace out trajectories in the (A, R) plane of Fig. 4, all of which will eventually intersect the line of existence. To calculate these trajectories, begin by writing Eq. (D4) for $A(t)$ and $R(t)$, obtaining $[A(t) - A_\infty] = \gamma_A [E(t) - E_\infty]^{\rho_A}$ and $[R(t) - R_\infty] = \gamma_R [E(t) - E_\infty]^{\rho_R}$, respectively. Substituting the first into the second to eliminate the energy, we obtain

$$R(t) = R_\infty + \gamma_{RA}[A(t) - A_\infty]^{\rho_{RA}}, \tag{31}$$

where $\gamma_{RA} \equiv \gamma_R/\gamma_A^{\rho_{RA}}$ and $\rho_{RA} \equiv \rho_R/\rho_A$. Note that when $A = A_\infty$, $R = R_\infty$.

Since each possible trajectory will intersect the line of existence, every point along the line of existence is a point along some trajectory. Thus, we can choose an arbitrary point on this line (which we will call the "reference point") and use its coordinates, labeled (A_r, R_r), to calculate all of the dynamical exponents (ρ_A, ρ_R, $\rho_{\dot{E}}$, ρ_ω, ρ_η, etc.) associated with the trajectory that intersects that point. Equation (D12), reproduced below, was evaluated numerically for $X = \rho_{\dot{E}}$ and $X = \rho_A$, respectively:

$$\rho_X = \frac{(2 + \frac{\partial \nu_\eta}{\partial \nu_E})\frac{\partial \nu_X}{\partial \nu_E} + (\frac{\partial \nu_\eta}{\partial \nu_A} - 2)\frac{\partial \nu_X}{\partial \nu_A}}{(2 + \frac{\partial \nu_\eta}{\partial \nu_E})}. \tag{32}$$

Figure 6 shows the results for the exponents $g \equiv \rho_{\dot{E}} - 1$ (top curve) and ρ_A (bottom curve) as a function of A_r.

Given values for ρ_X, we can calculate γ_X by evaluating each side of Eq. (D4) at the reference point (wherein X assumes the value $X_r = X[A_r, R_r]$) and solving for γ_X, obtaining

$$\gamma_X = \frac{X_r - X_\infty}{(E_r - E_\infty)^{\rho_X}}. \tag{33}$$

Figure 7 shows the results of such a calculation for $\gamma_{\dot{E}}$ (top graph) and γ_A (bottom graph).

Having computed ρ_X and γ_X for the parameters A and R allows us to calculate the coefficients in Eq. (31) for each trajectory [i.e., compute Eqs. (32) and (33) for various reference points along the line of existence]. The result of this is shown in Fig. 8 for selected trajectories. Note that

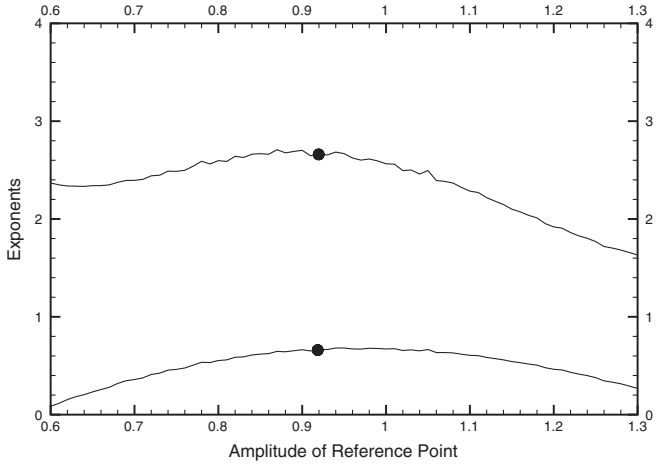

FIG. 6. Analytical calculation of $g = \rho_{\dot{E}} - 1$ (top curve) and ρ_A (bottom curve) using Eq. (32), plotted against the reference amplitude A_r along the line of existence. This gives the spectrum of possible values of g and ρ_A across the various oscillons in this system. The dots mark the theoretical values of $g \simeq 2.67$ and $\rho_A \simeq .66$ assumed by the longest-lived oscillon, which has $A_r \simeq .92$ (thicker line in Fig. 8).

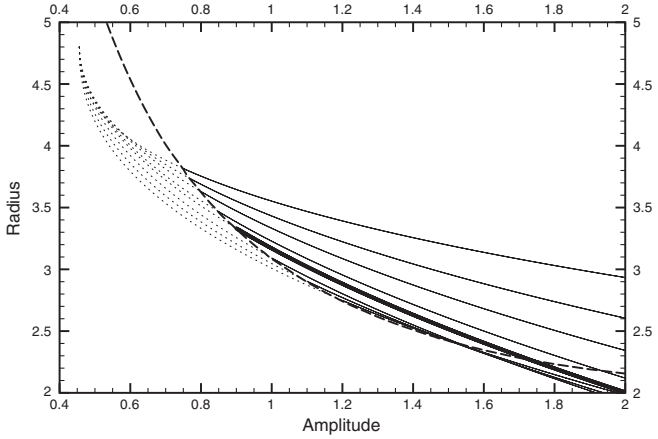

FIG. 8. Various oscillon trajectories. Note that they all tend to the attractor point but intersect the line of existence (dashed line) before doing so. The thicker trajectory marks the longest-lived oscillon (it intersects the line of existence at $A_r \simeq .92$ and $R_r \simeq 3.25$).

they all asymptotically tend toward the attractor point but intersect the line of existence before doing so.

As an example, consider the trajectory which intersects the line of existence at $A_r \simeq .92$ [this will be shown to correspond to the longest-lived oscillon in the system of Eq. (1)]. From Figs. 6 and 7, we have $g \simeq 2.67$ and $\gamma_{\dot{E}} \simeq 2.0 \times 10^{-6}$. If this oscillon were initiated at an energy of $E_i \simeq 82.5$ (which will be the case for the numerical simulation we will be comparing to), then Eq. (25) for that

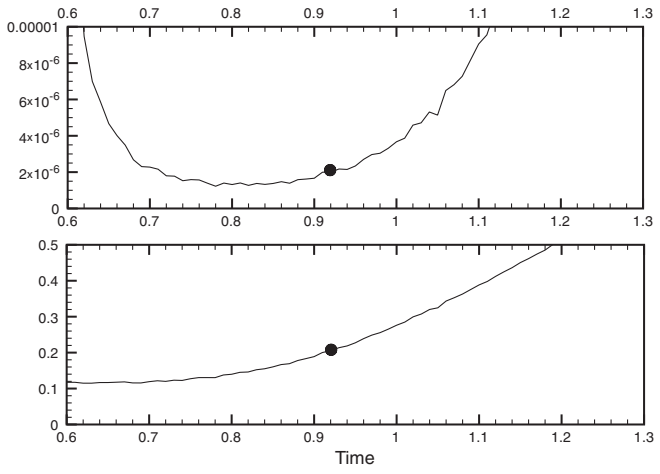

FIG. 7. Analytical calculation of $\gamma_{\dot{E}}$ (top graph) and γ_A (bottom graph) using Eq. (33), plotted against the reference amplitude A_r along the line of existence. This gives the spectrum of possible values of $\gamma_{\dot{E}}$ and γ_A across the various oscillons in this system. The dots serve to mark the theoretical values of $\gamma_{\dot{E}} \simeq 2.0 \times 10^{-6}$ and $\gamma_A \simeq .21$ assumed by the longest-lived oscillon, which has $A_r \simeq .92$ (thicker line in Fig. 8).

oscillon becomes

$$E(t) \simeq 37.69 + \frac{44.8}{[1 + (.136)t]^{.375}}, \tag{34}$$

which, for times $t \gtrsim 100$ is approximately

$$E(t) - E_\infty \simeq \frac{94.77}{t^{.375}}. \tag{35}$$

Since the decay energy for this oscillon is $E_D = E_r = E_r(A_r, R_r) \simeq 41.0963$, Eq. (28) yields

$$\mathcal{T}_{\text{life}} \simeq \frac{1}{[2.0 \times 10^{-6}][2.67]} \frac{1}{[41.10 - 37.69]^{2.67}} \simeq 7100. \tag{36}$$

Given Eq. (34), we can write, for example, an expression for the oscillon amplitude as a function of time. From Figs. 6 and 7, we have $\rho_A \simeq .67$ and $\gamma_A \simeq .21$. Combining this information with $[A - A_\infty] = \gamma_A[E - E_\infty]^{\rho_A}$ and Eq. (34), we have

$$A(t) \simeq .456 + \frac{2.58}{[1 + (.136)t]^{.249}}. \tag{37}$$

Carrying out the above calculations for several trajectories along the line of existence and plotting the lifetime vs A_r, R_r, and E_r, results in Figs. 9 and 10, respectively. Figure 9 shows the analytical decay amplitude and radius as a function of lifetime (dashed lines) plotted against several long-lived and short-lived oscillons, with excellent agreement: oscillons decay as they cross the coordinates specified by the line of existence. Figure 10 shows the computed lifetime as a function of decay energy ($E_D = E_r$), reproducing the maximum lifetime on the order of 10^4 which is characteristic of oscillons in this system. The figure compares the analytical computation of lifetime (continuous line) with the numerical results (dashed

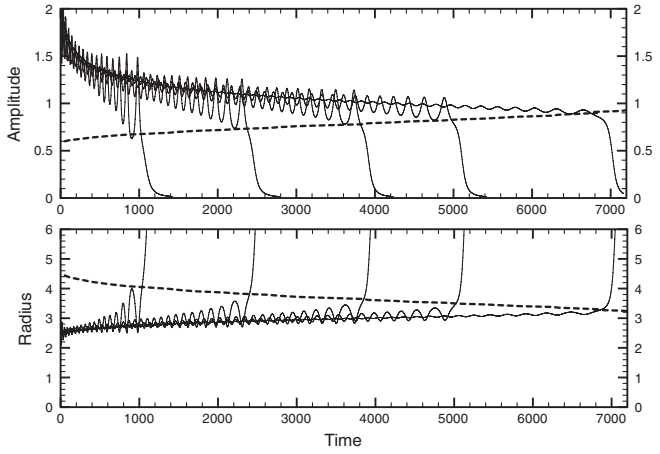

FIG. 9. Analytical results for critical values of the amplitude (top) and radius (bottom) along the line of existence (dashed lines) as a function of lifetime are plotted with several examples of short-and long-lived oscillons, all with initial amplitudes $A_0 = 2$. From left to right, the initial radii for the oscillons are 2.35, 2.41, 2.53, 2.65, and 2.86. It is quite clear that the oscillons decay as they cross the critical values computed analytically.

line). The small disparity in the center of the peak (of order $\sim$6%) is probably due to the Gaussian *ansatz* we use to describe oscillon configurations.

As was done in Eqs. (34) and (37), our method allows us to investigate an oscillon evolving along a particular trajectory in detail. As an example, we consider the longest-lived oscillon in this model, obtained with the initial parameters ($A_0 = 2$; $R_0 = 2.86$). Using the information from the curve in Fig. 10, we can find the trajectory whose lifetime corresponds to this oscillon ($\mathcal{T}_{\rm life} \simeq 7100$), marked as the thicker line in Fig. 8 [the coordinates of

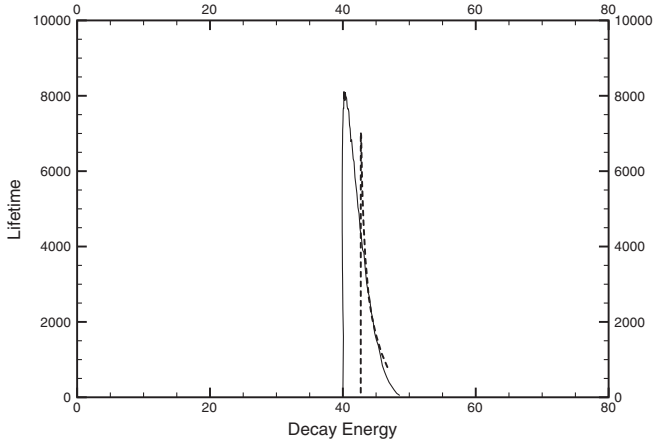

FIG. 10. Oscillon lifetimes vs decay energy $E_D = E_r$. Solid curve is theoretical, dashed line is numerical. The theoretical curve (with an error of $\sim$6% in the horizontal positioning of the peak) correctly predicts the shape of the distribution and that there exists a maximum lifetime in this system on the order of $\sim 10^4$.

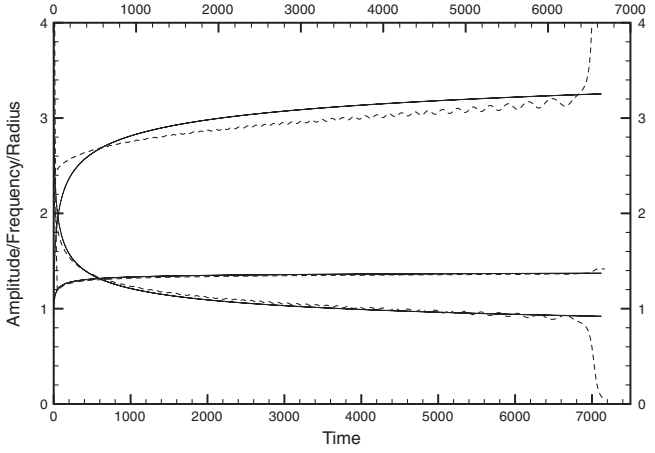

FIG. 11. Comparison of theoretical (continuous line) vs numerical (dashed line) radius (top), frequency (middle), and amplitude (bottom) for an oscillon with initial conditions ($A_0 = 2$, $R_0 = 2.86$), showing very good agreement [theoretical results are computed with $(A_r, R_r) \simeq (.92, 3.25)$].

the reference (or decay) point are $A_r \simeq .92$ and $R_r \simeq 3.25$]. We then use Eqs. (32) and (33) to calculate ρ_X and γ_X for any parameter of interest. Then, combining these values with Eqs. (25) and (D4), we can compute the amplitude [Eq. (37)], radius, frequency, energy Eq. (34)], and radiation rate as functions of time and compare the results with the numerical values. The results are plotted in Figs. 11–13, showing excellent agreement. We can also plot the theoretical prediction for the trajectory of this oscillon in the (A, R) plane (shown by the thicker line in Fig. 8), and compare it to the numerical value, as shown in Fig. 14.

In the next section, we will complete the characterization of this system by deriving an expression for the frequency of the superimposed oscillation observed in, for example, Fig. 9, which seems to be connected with

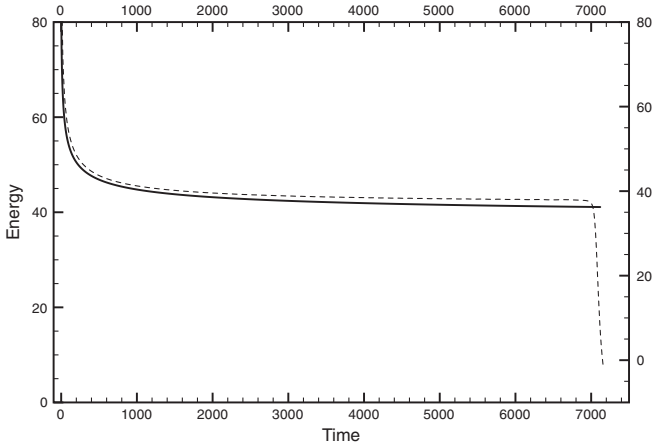

FIG. 12. Comparison of theoretical (continuous line) vs numerical (dashed line) values for the energy of the longest-lived oscillon, obtained with initial conditions ($A_0 = 2$, $R_0 = 2.86$) showing excellent agreement [$(A_r, R_r) \simeq (.92, 3.25)$].

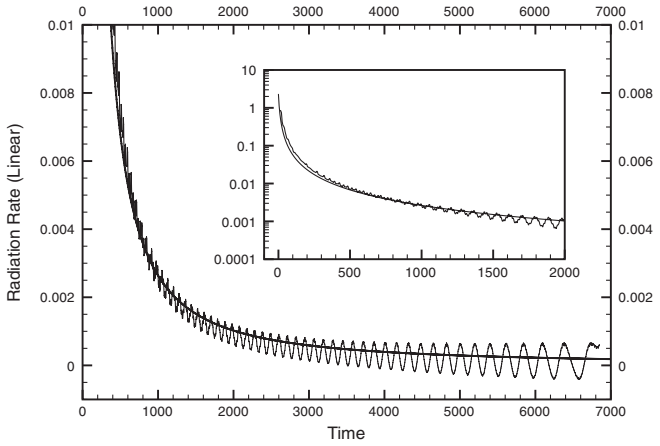

FIG. 13. Comparison of theoretical (continuous line) vs numerical (wavy line) radiation rate for an oscillon with initial conditions ($A_0 = 2$, $R_0 = 2.86$), showing excellent agreement. The inset, which is plotted on a log scale, makes it clear that the theory correctly reproduces the rapid initial drop in radiation rate over many orders of magnitude; the linear scale on the larger graph shows that the theory correctly reproduces the extremely small (but finite) radiation rate towards the end of the oscillon's life [$(A_r, R_r) \simeq (.92, 3.25)$].

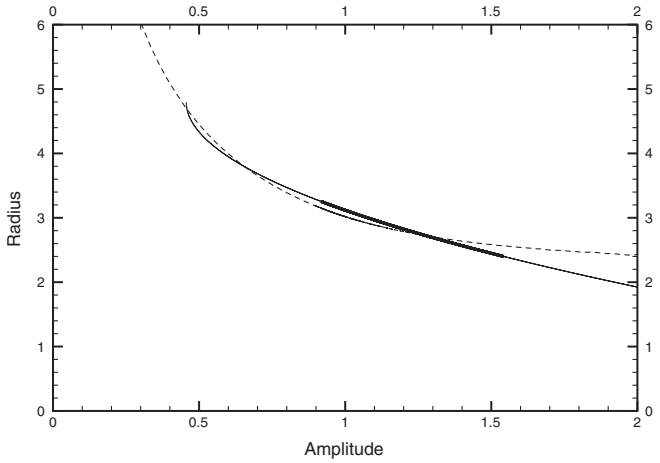

FIG. 14. Comparison of theoretical trajectory (solid curve) vs numerical trajectory (dashed curve) for the longest-lived oscillon ($A_0 = 2$, $R_0 = 2.86$), showing very good agreement during the more stable phase of the oscillon's life ($A \lesssim 1.5$). The great increase in density of data points in the dashed line in the range $.9 \lesssim A \lesssim 1.5$ is due to the prolonged period of time spent in this region by the oscillon (i.e., the ''plateau'' phase). The end point where the dashed line again becomes dashed ($A \simeq .9$, $R \simeq 3.2$) signals the numerical decay point of the oscillon. The thick segment of the solid line highlights the portion of the theoretical trajectory during the low-radiation plateau phase; the end of the thick segment $(A_r, R_r) \simeq (.92, 3.24)$ marks the theoretical decay point, showing very good agreement. It is interesting to note that, even after the oscillon decay at $A \simeq .9$, the remaining field configuration continues to tend to the attractor point at $(A_\infty, R_\infty) \simeq (.456, 4.79)$, as does the theoretical curve.

the oscillon decay process: the larger the amplitude of the superimposed oscillation, the shorter the lifetime.

IV. ANALYSIS OF OSCILLON STABILITY AS A FUNCTION OF TIME

Recall from the first chapter that the three conditions representing an oscillon before decay, at the point of decay, and after decay, respectively, are:

$$\omega_{\rm gap} > \Gamma_{\rm lin}; \qquad \omega_{\rm gap} = \Gamma_{\rm lin}; \qquad \omega_{\rm gap} < \Gamma_{\rm lin}. \tag{38}$$

In this section, we seek to investigate the concept of oscillon stability in more depth. In doing so, we will obtain a more general formulation of Eq. (38) which will provide a precise measure of the oscillon's stability when $\omega_{\rm gap} \neq \Gamma_{\rm lin}$. We will then see that an expression for the frequency of the superimposed oscillation seen in Fig. 9, which is clearly related to stability, will naturally emerge.

In deriving the equations governing the radiation rate and lifetime in the previous sections, we made the simplifying assumption that the oscillons under study are long-lived. Mathematically, this assumption is employed in approximating the series expansion in Eq. (B7) by its first term, yielding Eq. (B8). The more stable the oscillon, the smaller a given term in the series expansion will be relative to the term before it.

Let ν_n denote the magnitude of the nth term in the series of Eq. (B7). In this section, instead of assuming that $\nu_n \gg \nu_{n+1}$, we will compute the fractional difference between two adjacent terms and take the result to be a natural measure of the stability of the oscillon.

Define the (dimensionless) stability function Σ from two adjacent terms in the series of Eq. (B7) as

$$\Sigma \equiv \frac{\nu_n - \nu_{n+1}}{\nu_n}. \tag{39}$$

When the oscillon is highly stable, $\nu_n \gg \nu_{n+1}$, and $\Sigma \to 1$; conversely, as $\nu_{n+1} \to \nu_n$ [causing the series in Eq. (B7) to fail to converge] then $\Sigma \to 0$. In Appendix E [see Eq. (E7)] it is shown that, for any value of n,

$$\Sigma = 1 - \left(\frac{\Gamma_{\rm nl}}{\omega_{\rm gap}}\right)^2. \tag{40}$$

Equation (40) is referred to as the stability function; as would be expected, it involves the ratio between $\omega_{\rm gap}$ and $\Gamma_{\rm nl}$. Using Eq. (29) for $\Gamma_{\rm nl}$, we can plot Eq. (40) for the longest-lived oscillon [using Eqs. (32) and (33)]. This is shown in the top graph of Fig. 15. The extreme closeness of Σ to unity for most of the oscillon's life, when compared to Eq. (39), verifies that we are quite justified in assuming $\nu_n \gg \nu_{n+1}$.

The minimum stability allowed at a given time, $\Sigma_{\rm min}$, is attained when $\Gamma_{\rm nl}$ is at its maximum, namely, when $\Gamma_{\rm nl} = \Gamma_{\rm lin}$,

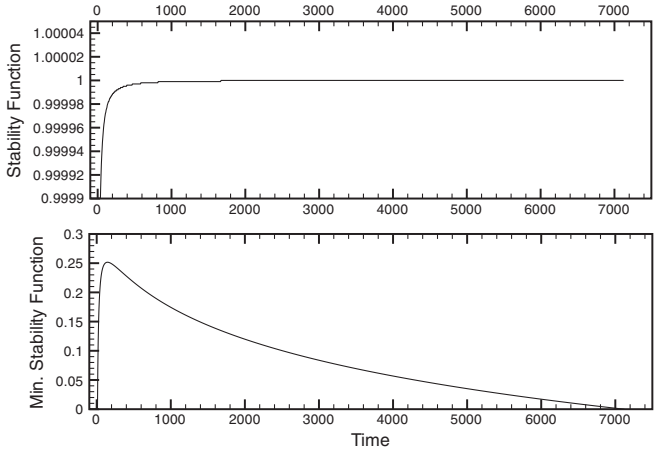

FIG. 15. The top graph shows the theoretical calculation of Σ vs time and the bottom shows $\Sigma_{\rm min}$, both for the oscillon with $(A_r, R_r) \simeq (.92, 3.25)$. The stability measured by Σ is clearly related to the radiation rate of the oscillon: this kind of stability increases in time, since the radiation rate decreases. On the other hand, the stability measured by $\Sigma_{\rm min}$ is related to the resistance of the oscillon to decay: this kind of stability decreases in time as the oscillon moves closer to the line of existence.

$$\Sigma_{\rm min} = 1 - \left(\frac{\Gamma_{\rm lin}}{\omega_{\rm gap}}\right)^2. \tag{41}$$

Now note that the conditions in Eq. (38) can be written in terms of $\Sigma_{\rm min}$ as

$$\Sigma_{\rm min} > 0; \qquad \Sigma_{\rm min} = 0; \qquad \Sigma_{\rm min} < 0, \tag{42}$$

respectively. In the bottom graph of Fig. 15, we plot $\Sigma_{\rm min}$ for the longest-lived oscillon [again, using Eqs. (32) and (33) and with $\Gamma_{\rm lin}$ given by Eq. (5)].

It is clear that one can interpret the stability Σ as a measure of the radiation rate of the oscillon: the radiation rate decreases in time, so the stability *increases*. On the other hand, $\Sigma_{\rm min}$ measures the resistance of the oscillon against spontaneous decay: as the oscillon evolves and approaches the line of existence, this kind of stability *decreases*.

We will now write the conditions in Eqs. (38) and (42) in a third and final form. First, observe that we can write $\Sigma_{\rm min}$ as

$$\Sigma_{\rm min} = \left(\frac{\omega_{\rm mod}}{\omega_{\rm gap}}\right)^2, \tag{43}$$

where

$$\omega_{\rm mod} \equiv \sqrt{\omega_{\rm gap}^2 - \Gamma_{\rm lin}^2}. \tag{44}$$

In terms of $\omega_{\rm mod}$, the conditions in Eq. (42) become

$$\omega_{\rm mod} \in \Re, \neq 0; \qquad \omega_{\rm mod} = 0; \qquad \omega_{\rm mod} \in \Im, \tag{45}$$

respectively. In other words, if we consider the quantity $B(t) \equiv e^{i\omega_{\rm mod} t}$, then the real part of $B(t)$ before the decay, at the decay point, and after the decay are

$$B(t) = \cos(\sqrt{\omega_{\rm gap}^2 - \Gamma_{\rm lin}^2}\, t); \qquad B(t) = 1; \qquad B(t) = e^{\pm\Gamma_{\rm lin} t}, \tag{46}$$

respectively, where the last condition follows since, after the decay is initiated, $\omega_{\rm gap}$ tends to zero, making $\omega_{\rm mod}$ tend to $\pm i\Gamma_{\rm lin}$.

Therefore, we can conclude that $\omega_{\rm mod}$ is a special frequency associated with the decay of the oscillon whose value decreases in time and, at a certain point, becomes imaginary, signaling the oscillon's final demise with time scale on the order of the linear decay width [Eq. (46)]. In fact, as mentioned previously, such a phenomenon is commonly observed in, for example, Fig. 9. Specifically, there exists a modulation oscillation whose frequency tends to decrease as time progresses, until, at a certain point, the oscillon decays with width $\sim\Gamma_{\rm lin}$.

In Fig. 16, we plot the period

$$\mathcal{T}_{\rm decay} \equiv \frac{2\pi}{\omega_{\rm mod}} = \frac{2\pi}{\sqrt{\omega_{\rm gap}^2 - \Gamma_{\rm lin}^2}}, \tag{47}$$

along with the numerically measured period of the superimposed oscillation. As shown, $\mathcal{T}_{\rm decay}$ quite accurately reproduces this frequency.

In conclusion, we now have three separate (yet equivalent) formulations of the condition for oscillon decay. The first says that the nonlinear and linear peaks must significantly overlap [Eqs. (38)]. The second says that the measure of oscillon stability must fall to zero [Eqs. (42)]. The last states that the modulation frequency $\omega_{\rm mod}$ must become imaginary [Eqs. (45)].

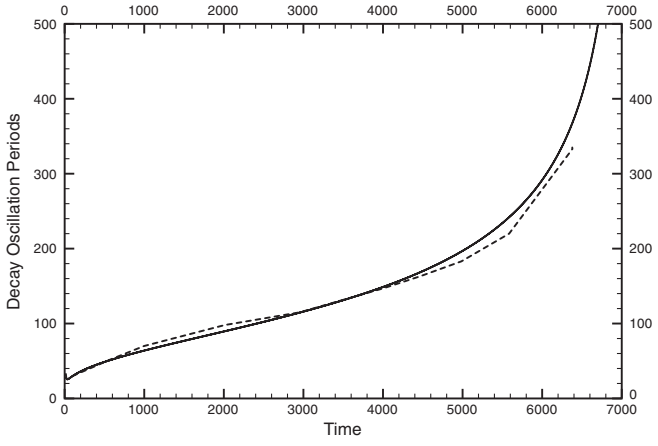

FIG. 16. The solid curve is the theoretical calculation of $\mathcal{T}_{\rm decay}$ for $(A_r, R_r) \simeq (.92, 3.25)$. The dashed curve is the numerically measured period of the superimposed oscillation, showing very good agreement.

V. THE FOUR OSCILLON TIME SCALES

We will now review the four time scales associated with oscillons encountered in our theory. They are:

$$\mathcal{T}_{\text{relax}} = -\frac{E - E_\infty}{\dot{E}} = \frac{1}{\gamma_{\dot{E}}[E - E_\infty]^g} = \Gamma_E^{-1}, \tag{48}$$

$$\mathcal{T}_{\text{decay}} = \frac{2\pi}{\sqrt{\omega_{\text{mod}}^2 - \Gamma_{\text{lin}}^2}}, \tag{49}$$

$$\mathcal{T}_{\text{linear}} \sim \omega_{\text{mass}} R^2, \tag{50}$$

$$\mathcal{T}_{\text{osc}} = \frac{2\pi}{\omega_{\text{nl}}}. \tag{51}$$

The first, $\mathcal{T}_{\text{relax}}$, is the relaxation time of the oscillon and is typically the longest time scale present. This is the time scale over which the oscillon experiences significant change. Its net value expresses the inverse rate of energy radiation, being thus largest where the oscillon radiates the least, as can be seen from the flatness of curves such as those in Fig. 11 and 12. This is linked to the lifetime by

$$\mathcal{T}_{\text{life}} = \frac{1}{\gamma_{\dot{E}} g} \frac{1}{[E_D - E_\infty]^g} = \frac{1}{g} \mathcal{T}_{\text{relax}}|_{E=E_D} \sim \mathcal{T}_{\text{relax}}|_{E=E_D}, \tag{52}$$

where we have used Eq. (28) and the fact that the dynamical exponents are typically of order unity (see Fig. 6).

The second time scale, $\mathcal{T}_{\text{decay}}$, is the period of the superimposed oscillations seen in the oscillon as a result of its motion towards the line of existence. The third is the decay time of an object in the linear theory [8]. The fourth, and shortest time scale, is the oscillation period of the oscillon.

The theoretical values of the four time scales are plotted in Fig. 17 vs time for the longest-lived oscillon. Note how, together, they span many orders of magnitude. It is the presence of these four widely different time scales in one single system that makes oscillons such intriguing objects to study.

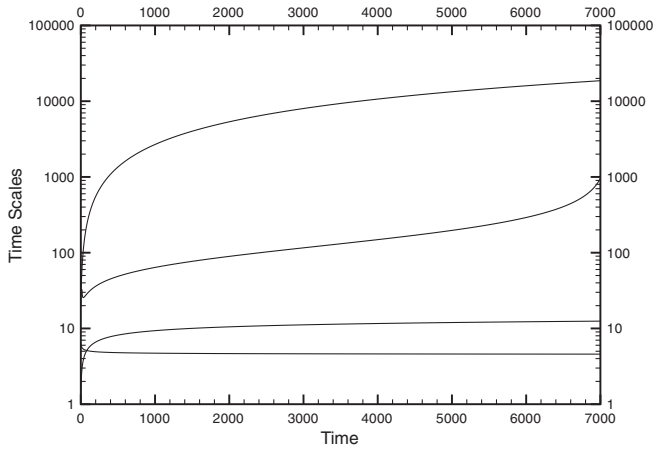

FIG. 17. The four oscillon time scales plotted over time. From top to bottom we have plotted $\mathcal{T}_{\text{relax}}$, $\mathcal{T}_{\text{decay}}$, $\mathcal{T}_{\text{linear}}$, and $\mathcal{T}_{\text{osc}}$. It can clearly be seen here that an oscillon is an object governed by multiple time scales spanning many orders of magnitude.

VI. CONCLUSIONS AND OUTLOOK

In this work, we expanded upon and improved our method to compute analytically the decay rate and lifetime of oscillonlike configurations [15]. Our approach relies on the comparison between the radiation spectrum of the nonlinear, oscillon-bearing, model and its linear limit. The radiation ultimately responsible for the oscillon decay is related to the overlap between the two spectra: the larger the overlap, the faster the decay. We have shown that in both $d = 2$ and $d = 3$ there is an attractor point in field configuration space and that oscillons may form as configurations evolve toward that point. In $d = 3$, we may think of oscillons as unstable but very long-lived perturbations about the attractor point. In $d = 2$, oscillons may be considered as perturbatively stable perturbations about the attractor point. All oscillon configurations are shown to migrate toward the attractor point as they evolve in time. However, in $d = 3$ this point lies below the oscillon's line of existence, and no oscillons in the models analyzed here, double-well potentials, are absolutely stable. It remains to be seen if it is possible to find models in $d = 3$ where oscillons are perturbatively stable. In $d = 2$, the situation is different: the attractor point lies within the oscillon region and our theory predict that they should be at least perturbatively stable or exceedingly long-lived. We can thus interpret the oscillons in symmetric double-well potentials as special types of perturbations about the attractor point: those in $d = 3$ are unstable but can be very long-lived, while those in $d = 2$ are perturbatively stable. Comparison with numerical results show that our method provides a very good quantitative description of these configurations. We remark that there are very few examples in the literature where analytical results provide a good description of time-dependent, nonperturbative phenomena in relativistic field theories in $d > 1$. We have also obtained a precise criterion to establish the stability of these configurations, as encapsulated in the oscillon stability function of Eq. (41).

It should be borne in mind that the assumptions used in this paper, although quite general, limit the applicability of the theory. First, it is known that the oscillon solution is not an exact Gaussian. Therefore, given that all quantitative predictions made by the theory are based on the Gaussian, all results will possess a slight error. The exact nature of this error is difficult to quantify; however, it should be small given that the oscillon (in the models studied here) is known to be well approximated by a Gaussian. Another

limitation of the theory lies in Eq. (D4). In the models studied in this paper, the core amplitudes of oscillons with shorter lifetimes oscillate with large amplitude about their mean value. (See, e.g., Fig. 9.) Since the energy $E(t)$ does not oscillate, it follows that it is not possible to state, for example, that $A(t) - A_\infty = \gamma_A (E - E_\infty)^{\rho_A}$, when the oscillation amplitude of the superimposed oscillon (or of the radius, $R(t)$) is large. Thus, our theory cannot make accurate predictions of the time dependence of individual parameters for oscillons which are relatively short-lived.

Given the generality of our method, we expect it to be extendable to many other models. For example, a simple next step would be to apply it to oscillons in asymmetric double-well potentials, where their longevity is expected to increase [6]. We currently are searching for models where oscillons in $d = 3$ may have an attractor point *above* the line of existence. The relative location of the attractor point with respect to the line of existence should serve as a general criterion to determine the longevity of time-dependent scalar field configurations in a variety of models, including those with more than one scalar field. Quite possibly, there may be models with two coupled fields that produce stable oscillons even in $d = 3$, at least in the sense that $\Sigma_{\min} \geq 1$. Another possible extension of the present results is the inclusion of gauge fields. As shown in Refs. [11,12], in both U(1) and SU(2)XU(1) models oscillons have not been seen to decay. The question of their absolute stability remains open and is of obvious interest. Finally, oscillons may play a key role in the dynamics of the early universe: they may be formed during preheating after inflation and delay thermalization; they may leave behind a gravitational-radiation signature; and they may contribute to the dark matter component of the cosmic energy density. We are currently investigating how to extend the current methods to an expanding cosmological background.

ACKNOWLEDGMENTS

We thank Noah Graham for many useful discussions and suggestions. This work was supported in part by a National Science Foundation Grant No. PHY-0757124.

APPENDIX A: LINEAR RADIATION DISTRIBUTION IN $d = 2$

We begin by expanding the Gaussian in eigenfunctions (zeroth-order bessel function of the first kind) of the two-dimensional, spherically-symmetric Klein-Gordon equation:

$$A(t)e^{-(\rho^2/R^2)} = \int_0^\infty b(k) J_0(k\rho) dk. \tag{A1}$$

Using the orthogonality relation

$$\int_0^\infty \rho J_0(k\rho) J_0(k'\rho) d\rho = \frac{1}{k}\delta(k - k'), \tag{A2}$$

we can invert Eq. (A1) to yield

$$b(k) = kA(t) \int_0^\infty J_0(k\rho) e^{-(\rho^2/R^2)} \rho d\rho. \tag{A3}$$

In [17], it is shown that integration gives

$$b(k) = \frac{R^2 A}{2} k e^{-R^2 k^2/4}. \tag{A4}$$

Note that this function has the same form as the corresponding one in $d = 3$. Hence the results in Eqs. (6) and (7) need not be recomputed. To obtain Γ_{lin} in $d = 2$ one could, in principle, solve the equation of motion as was done in $d = 3$; however, for our purposes it will be sufficient to determine this parameter numerically (by numerically integrating the linear Klein-Gordon equation in $d = 2$ with a Gaussian initial condition), yielding

$$\frac{1}{2}\Gamma_{\text{lin}} = \frac{1}{\mathcal{T}_{\text{linear}}} \simeq \frac{.848}{\omega_{\text{mass}} R^2} \simeq \frac{.6}{R^2}. \tag{A5}$$

APPENDIX B: DERIVATION OF NONLINEAR FREQUENCY PEAK

In this paper, we consider spherically-symmetric oscillons which can be accurately modeled by an oscillating field configuration whose spatial profile and amplitude of oscillation vary little over the course of an oscillation, i.e.,

$$\phi(r, t) \simeq A_c(t) P(r; R) \equiv A_{\text{osc}}(t) A(t) P(r; R), \tag{B1}$$

where ϕ is the field, r is radial position, t is time, $P(r)$ is the spatial profile of the oscillon normalized so that $P(r) = 1$ at the origin, R is a time-dependent measure of the spatial extent of the oscillon (i.e., the "radius") which is assumed to vary little over the period of a single oscillation, $A_c(t)$ is the time-dependent oscillon core $[\phi(0, t)]$, $A(t)$ is its time-dependent envelope of oscillation, and $A_{\text{osc}}(t)$ is an oscillating function which is normalized to an upper turning point of unity.

If the oscillon oscillates approximately harmonically, we can write

$$A_{\text{osc}}(t) \simeq \frac{\chi}{1 + \chi} + \frac{\cos(\omega_{\text{nl}} t)}{1 + \chi}, \tag{B2}$$

where ω_{nl} is the time-dependent frequency of the oscillon and χ is a dimensionless constant which accounts for a possible nonzero center of oscillation.

Now assume that we are interested in calculating the radiation rate of the oscillon at $t = 0$. Since the oscillon radiation rate depends only on the instantaneous properties of the oscillon, writing $\omega_{\text{nl}}(t) = \omega_{\text{nl}}(0)$ in Eq. (B2) will still yield the correct radiation rate at $t = 0$. Combining Eqs. (B1) and (B2) and taking the unitary cosine transform of A_c, we have

$$\mathcal{F}(\omega) = \sqrt{\frac{2}{\pi}}\int_0^\infty \cos(\omega t)A_c(t)dt$$
$$= \sqrt{\frac{2}{\pi}}\int_0^\infty \cos(\omega t)\cos(\omega_{\rm nl}(0))\frac{A(t)}{1+\chi}dt, \quad \text{(B3)}$$

where in the second step we have multiplied $A(t)$ by $A_{\rm osc}(t)$ in Eq. (B2) and dropped all terms except the one proportional to $\cos(\omega_{\rm nl}t)A(t)$ which will create a finite width peak centered at the oscillon frequency (all others are irrelevant and do not contribute to the radiation rate). We can rewrite Eq. (B3) as

$$\mathcal{F}(\omega) = \frac{1}{\sqrt{2\pi}}\int_0^\infty [\cos(\omega_+ t) + \cos(\omega_- t)]\frac{A(t)}{1+\chi}dt, \quad \text{(B4)}$$

where $\omega_+ \equiv \omega_{\rm nl} + \omega$ and $\omega_- \equiv \omega_{\rm nl} - \omega$. Since each of the two cosine terms above will contribute an identical peak (one centered at $+\omega_{\rm nl}$ and the other at $-\omega_{\rm nl}$) and both will contribute identically to the radiation rate, we can simply drop the one centered on $-\omega_{\rm nl}$ and multiple by two, yielding

$$\mathcal{F}(\omega) = \sqrt{\frac{2}{\pi}}\int_0^\infty \cos([\omega_{\rm nl} - \omega]t)\frac{A(t)}{1+\chi}dt. \quad \text{(B5)}$$

Now, since an oscillon's amplitude $A(t)$ tends to a finite value, denoted A_∞, as $t \to \infty$, we define $A_\Delta \equiv A(t) - A_\infty$ and write

$$\mathcal{F}(\omega) = \sqrt{\frac{2}{\pi}}\int_0^\infty \cos([\omega_{\rm nl} - \omega]t)\frac{(A_\Delta + A_\infty)}{1+\chi}dt$$
$$= \sqrt{\frac{2}{\pi}}\int_0^\infty \cos([\omega_{\rm nl} - \omega]t)\frac{A_\Delta}{1+\chi}dt, \quad \text{(B6)}$$

where we have dropped the transform of the A_∞ term since it will produce a delta function centered at $\omega_{\rm nl}$ which will not in anyway affect $\mathcal{F}(\omega)$ in the region of interest (the radiation zone).

To proceed, we use the fact (found by performing successive integration by parts) that, for a function $f(x)$ which tends to zero as $x \to \infty$,

$$\int_0^\infty \cos(sx)f(x)dx = \sum_{n=1}^\infty (-1)^n \frac{f^{(2n-1)}(0)}{s^{2n}}, \quad \text{(B7)}$$

where $f^{(m)}$ is the mth derivative of the function f. We apply Eq. (B7) to Eq. (B6) and note that, for a long-lived oscillon, the flatness of $A(t)$ implies that, for s in the tail, we need only keep the first term, yielding

$$\mathcal{F}(\omega) \simeq -\sqrt{\frac{2}{\pi}}\frac{\dot{A}}{1+\chi}\frac{1}{(\omega_{\rm nl} - \omega)^2}, \quad \text{(B8)}$$

where we have switched the evaluations at $t = 0$ to a general time t, since the above calculation can be applied to any physical time. Equation (B8) essentially states that when a peak associated with a decaying function has a very small width then the tail goes like $(\omega_{\rm nl} - \omega)^{-2}$.

It will be useful to note that $\mathcal{F}(\omega)$ in Eq. (B6) will be a peak whose width, denoted Γ_A, scales as

$$\Gamma_A \sim \left(\frac{A_\Delta}{1+\chi}\right)^{-1}\frac{d}{dt}\left(\frac{A_\Delta}{1+\chi}\right)\Big|_{t=t'} = \frac{\dot{A}}{A - A_\infty}., \quad \text{(B9)}$$

where we have used that χ is a constant, $A_\Delta \equiv A - A_\infty$, and A_∞ is a constant.

APPENDIX C: OVERLAP FUNCTION

Consider the overlap function $\Omega(\omega)$ in Eq. (17),

$$\Omega(\omega) = \alpha\mathcal{F}(\omega)b(\omega) \equiv \mathcal{F}(\omega)\tilde{b}(\omega). \quad \text{(C1)}$$

Since $\Omega(\omega)$ has dimension of amplitude per unit frequency [see Eq. (16)], as does $\mathcal{F}(\omega)$, it follows that $\tilde{b}(\omega)$ is dimensionless. Therefore, one can interpret $\tilde{b}(\omega)$ as a dimensionless coupling factor which modulates the distribution $\mathcal{F}(\omega)$. If the oscillon couples weakly to a certain mode, $\tilde{b}(\omega)$ will be small at that value of ω, etc.

Now, $\tilde{b}(\omega)$, which is proportional to the linear radiation distribution, will be a peak whose frequency of maximum coupling $\omega_{\rm max}$ is found by

$$\frac{d\tilde{b}}{d\omega}\Big|_{\omega=\omega_{\rm max}} = 0. \quad \text{(C2)}$$

Consider now that the largest-amplitude radiation wave which can be created by a driving force of frequency $\omega > \omega_{\rm mass}$ will be produced by driving at the frequency $\omega_{\rm max}$. However, the largest-amplitude radiation wave which can be created by a given driving force will have an amplitude on the order of the driving force itself (never larger). Therefore, at frequencies near $\omega_{\rm max}$, the amplitude of the radiation wave Ω will be roughly equal to the amplitude of the "driving force" $\mathcal{F}$. In other words, $\Omega(\omega_{\rm max}) \simeq \mathcal{F}(\omega_{\rm max})$, implying that $\tilde{b}(\omega_{\rm max}) \simeq 1$ from Eq. (C1). This leads to

$$\alpha \simeq \frac{1}{b(\omega_{\rm max})}, \quad \text{(C3)}$$

which, when combined with Eqs. (17) and (B8), yields

$$\Omega(\omega) \simeq -\sqrt{\frac{2}{\pi}}\frac{\dot{A}}{1+\chi}\frac{1}{(\omega_{\rm nl} - \omega)^2}\frac{b(\omega)}{b(\omega_{\rm max})}. \quad \text{(C4)}$$

For example, in the system given by Eq. (1), where $b(\omega)$ is given by Eq. (6), $\omega_{\rm max} = \sqrt{2 + 2/R^2}$. This leads to $\alpha = e^{1/2}R/\sqrt{2}$ and, when combined with Eq. (17), gives

$$\Omega(\omega) = -\frac{R}{\sqrt{\pi}}\frac{\dot{A}}{1+\chi}\frac{(\omega^2 - 2)^{(1/2)}}{(\omega_{\rm nl} - \omega)^2}e^{(1/2)-((R^2)/4).(\omega^2-2)}. \quad \text{(C5)}$$

This function is plotted in the inset of Fig. 5 for typical values of the parameters in the system given by Eq. (1) in $d = 3$. Equation (C5) gives the distribution (amplitude per unit frequency) of the radiation wave emitted by the oscillon in the vicinity of a time t. Its integral with respect to frequency gives the total amplitude of the radiation wave emitted by the oscillon, denoted $\mathcal{A}$.

Given an expression for $\Omega(\omega)$, δ and $\omega_{\rm rad}$ can then be given by

$$\Omega'(\omega_{\rm rad}) = 0; \qquad \frac{1}{2}\delta = \left[\frac{\int(\omega - \omega_{\rm rad})^2\Omega(\omega)d\omega}{\int\Omega(\omega)d\omega}\right]^{(1/2)}, \tag{C6}$$

where the prime denotes a derivative with respect to ω.

APPENDIX D: DYNAMICAL EXPONENTS

The time dependence of the oscillon and all of the various parameters which describe it is due to a *single* physical mechanism, namely, the emission of radiation. If the radiation rate is high (low), all parameters will change rapidly (slowly). In other words, the general nature of the time dependence of a parameter will follow that of any other parameter.

In analogy with Eq. (B9), define

$$\Gamma_X \propto \frac{\dot{X}}{X - X_\infty} \tag{D1}$$

which can be interpreted as the decay width for the parameter X. Now consider the generic parameters $X(t)$ and $Y(t)$ (which could represent amplitude, radius, frequency, etc.). Intuitively, we can say that the time scales Γ_X and Γ_Y associated with the rates of change of the parameters $X(t)$ and $Y(t)$, respectively, are to be proportional,

$$\Gamma_X \propto \Gamma_Y \tag{D2}$$

for any parameters $X(t)$, $Y(t)$ (i.e., if $X(t)$ slows down by a factor of 2, then so will every other parameter). We can then write, quite generally, $\Gamma_X \propto \Gamma_E$ for any parameter X, where E denotes energy. Combining this with Eq. (D1), yields

$$\frac{\dot{X}}{X(t) - X_\infty} = \rho_X \frac{\dot{E}}{E(t) - E_\infty}, \tag{D3}$$

where ρ_X denotes the proportionality constant. Integrating both sides of Eq. (D3), yields

$$[X(t) - X_\infty] = \gamma_X[E(t) - E_\infty]^{\rho_X}, \tag{D4}$$

where γ_X is the constant of integration.

We will now derive an expression for the general exponent ρ_X. First, define the new variable

$$\nu_X \equiv \ln(X - X_\infty), \tag{D5}$$

which we will henceforth employ in this Appendix, instead of X, to describe the oscillon. When combined with Eq. (D3), this gives

$$\rho_X = \frac{d\nu_X}{d\nu_E}. \tag{D6}$$

During the evolution of an oscillon, the change in the coordinate ν_X is given by

$$d\nu_X = \nabla\nu_X \cdot d\vec{\nu}, \tag{D7}$$

where $d\vec{\nu}$ is a differential vector which lies tangent to the trajectory of the oscillon in $\vec{\nu}$ space and $\nabla\nu_X$ is the vector gradient of ν_X whose direction lies perpendicular to the "level" curves associated with ν_X. To calculate $d\vec{\nu}$, we note that, by virtue of the attractorlike nature of oscillons, the oscillon will evolve according to a trajectory which runs perpendicular to the level curves associated with the radiation rate. Mathematically, we can write

$$\nabla\nu_{\dot{E}} \times d\vec{\nu} = 0. \tag{D8}$$

To proceed, we will make use of our initial assumption in Eq. (B1) that the oscillon (and hence any oscillon parameter X or ν_X) can be taken to be a function of 2 degrees of freedom. These 2 degrees of freedom can be arbitrarily chosen to be any two independent oscillon parameters. Choosing the coordinate pair $\vec{\nu} = (\nu_E, \nu_A)$, Eq. (D8) becomes

$$\frac{\partial\nu_{\dot{E}}}{\partial\nu_E}d\nu_A - \frac{\partial\nu_{\dot{E}}}{\partial\nu_A}d\nu_E = 0. \tag{D9}$$

Combining this with Eq. (D7) and dividing by $d\nu_E$, we have

$$\frac{d\nu_X}{d\nu_E} = \frac{\frac{\partial\nu_{\dot{E}}}{\partial\nu_E}\frac{\partial\nu_X}{\partial\nu_E} + \frac{\partial\nu_{\dot{E}}}{\partial\nu_A}\frac{\partial\nu_X}{\partial\nu_A}}{\frac{\partial\nu_{\dot{E}}}{\partial\nu_E}}. \tag{D10}$$

Combining Eqs. (24) and (D6), we have

$$\rho_{\dot{E}} = 2 - 2\rho_A + \rho_\eta = \frac{d}{d\nu_E}(2\nu_E - 2\nu_A + \nu_\eta) = \frac{d}{d\nu_E}\nu_{\dot{E}}, \tag{D11}$$

which implies that, up to a constant, $\nu_{\dot{E}} = 2\nu_E - 2\nu_A + \nu_\eta$. Substitution of this expression for $\nu_{\dot{E}}$ into Eq. (D10) and combining with Eq. (D6), yields the desired result:

$$\rho_X = \frac{(2 + \frac{\partial\nu_\eta}{\partial\nu_E})\frac{\partial\nu_X}{\partial\nu_E} + (\frac{\partial\nu_\eta}{\partial\nu_A} - 2)\frac{\partial\nu_X}{\partial\nu_A}}{(2 + \frac{\partial\nu_\eta}{\partial\nu_E})}. \tag{D12}$$

APPENDIX E: DERIVATION OF STABILITY FUNCTION

From Eq. (D4) it can be shown by differentiating that,

$$\dot{X} \propto (X - X_\infty)^a, \tag{E1}$$

where $a \equiv 1 + \frac{g}{\rho_X}$. By further differentiating, it can be

shown that

$$\frac{X^{(m)}}{X^{(n)}} \propto \left(\frac{\dot{X}}{X - X_\infty}\right)^{m-n} = \Gamma_X^{m-n}, \tag{E2}$$

where $X^{(m)}$ denotes the mth derivative of X with respect to time. Now, from Eq. (39),

$$\Sigma \equiv \frac{\nu_n - \nu_{n+1}}{\nu_n} = 1 - \frac{\nu_{n+1}}{\nu_n}. \tag{E3}$$

From Eq. (B7) we have,

$$\frac{\nu_n}{\nu_{n+1}} = \frac{s^2}{f^{(2n+1)}/f^{(2n-1)}} = \frac{(\omega - \omega_{\rm nl})^2}{A^{(2n+1)}/A^{(2n-1)}}, \tag{E4}$$

where we have used Eq. (B8) and the fact that χ is a constant. Combining Eq. (E4) with Eq. (E2) (in the case that $X = A$), we have

$$\frac{\nu_n}{\nu_{n+1}} \propto \left(\frac{\omega - \omega_{\rm nl}}{\Gamma_{\rm nl}}\right)^2 = \beta\left(\frac{\omega - \omega_{\rm nl}}{\Gamma_{\rm nl}}\right)^2, \tag{E5}$$

where β is a proportionality constant and we have used that $\Gamma_{\rm nl} = \Gamma_A$. Combining Eq. (E5) with Eq. (E3), we have

$$\Sigma = 1 - \frac{1}{\beta}\left(\frac{\Gamma_{\rm nl}}{\omega - \omega_{\rm nl}}\right)^2. \tag{E6}$$

Equation (E6) is a function of ω; to determine the appropriate value of ω, we note that, if $\Gamma_{\rm nl}$ were to attain its maximum value of $\Gamma_{\rm lin}$ and if $\Gamma_{\rm lin} = \omega_{\rm gap}$, the oscillon would decay; therefore, $\Sigma = 0$ when $\Gamma_{\rm nl} = \Gamma_{\rm lin} = \omega_{\rm gap}$. This implies that $\beta(\omega - \omega_{\rm nl})^2 = \omega_{\rm gap}^2$. Substitution of this into Eq. (E6) yields the desired result of

$$\Sigma = 1 - \left(\frac{\Gamma_{\rm nl}}{\omega_{\rm gap}}\right)^2. \tag{E7}$$

[1] R. Rajamaran, *Solitons and Instantons* (North-Holland, Amsterdam, 1987).
[2] G. H. Derrick, J. Math. Phys. (N.Y.) **5**, 1252 (1964).
[3] A. Vilenkin and E. P. S. Shellard, *Cosmic Strings and Other Topological Defects* (Cambridge University Press, Cambridge, 1994).
[4] S. Coleman, Nucl. Phys. **B262**, 263 (1985).
[5] R. Friedberg, T. D. Lee, and A. Sirlin, Phys. Rev. D **13**, 2739 (1976); T. D. Lee and Y. Pang, Phys. Rep. **221**, 251 (1992).
[6] M. Gleiser, Phys. Rev. D **49**, 2978 (1994).
[7] I. L. Bogolubsky and V. G. Makhankov, Pis'ma Zh. Eksp. Teor. Fiz. **24**, 15 (1976) [JETP Lett. **24**, 12 (1976)].
[8] E. J. Copeland, M. Gleiser, and H.-R. Müller, Phys. Rev. D **52**, 1920 (1995).
[9] M. Gleiser and A. Sornborger, Phys. Rev. E **62**, 1368 (2000); M. Hindmarsh and P. Salmi, Phys. Rev. D **74**, 105005 (2006); **77**, 105025 (2008).
[10] M. Gleiser, Phys. Lett. B **600**, 126 (2004); P. M. Saffin and A. Tranberg, J. High Energy Phys. 01 (2007) 030.
[11] M. Gleiser and J. Thorarinson, Phys. Rev. D **76**, 041701(R) (2007); **79**, 025016 (2009).
[12] E. Farhi, N. Graham, V. Khmeani, R. Markov, and R. Rosales, Phys. Rev. D **72**, 101701 (2005); N. Graham, Phys. Rev. Lett. **98**, 101801 (2007); **98**, 189904(E) (2007).
[13] N. Graham and N. Stamatopoulos, Phys. Lett. B **639**, 541 (2006); E. Farhi *et al.*, Phys. Rev. D **77**, 085019 (2008); M. Gleiser, Int. J. Mod. Phys. D **16**, 219 (2007).
[14] G. Fodor, P. Forgács, P. Grandclément, and I. Rácz, Phys. Rev. D **74**, 124003 (2006); G. Fodor, P. Forgács, Z. Horváth, and Á. Lukács, Phys. Rev. D **78**, 025003 (2008); G. Fodor, P. Forgács, Z. Horváth, and M. Mezei, Phys. Rev. D **79**, 065002 (2009); Phys. Lett. B **674**, 319 (2009).
[15] M. Gleiser and D. Sicilia, Phys. Rev. Lett. **101**, 011602 (2008).
[16] M. Gleiser and R. Howell, Phys. Rev. E **68**, 065203 (2003); M. Gleiser, B. Rogers, and J. Thorarinson, Phys. Rev. D **77**, 023513 (2008).
[17] G. N. Watson, *A Treatise on the Theory of Bessel Functions* (Cambridge University Press, Cambridge, 1962).